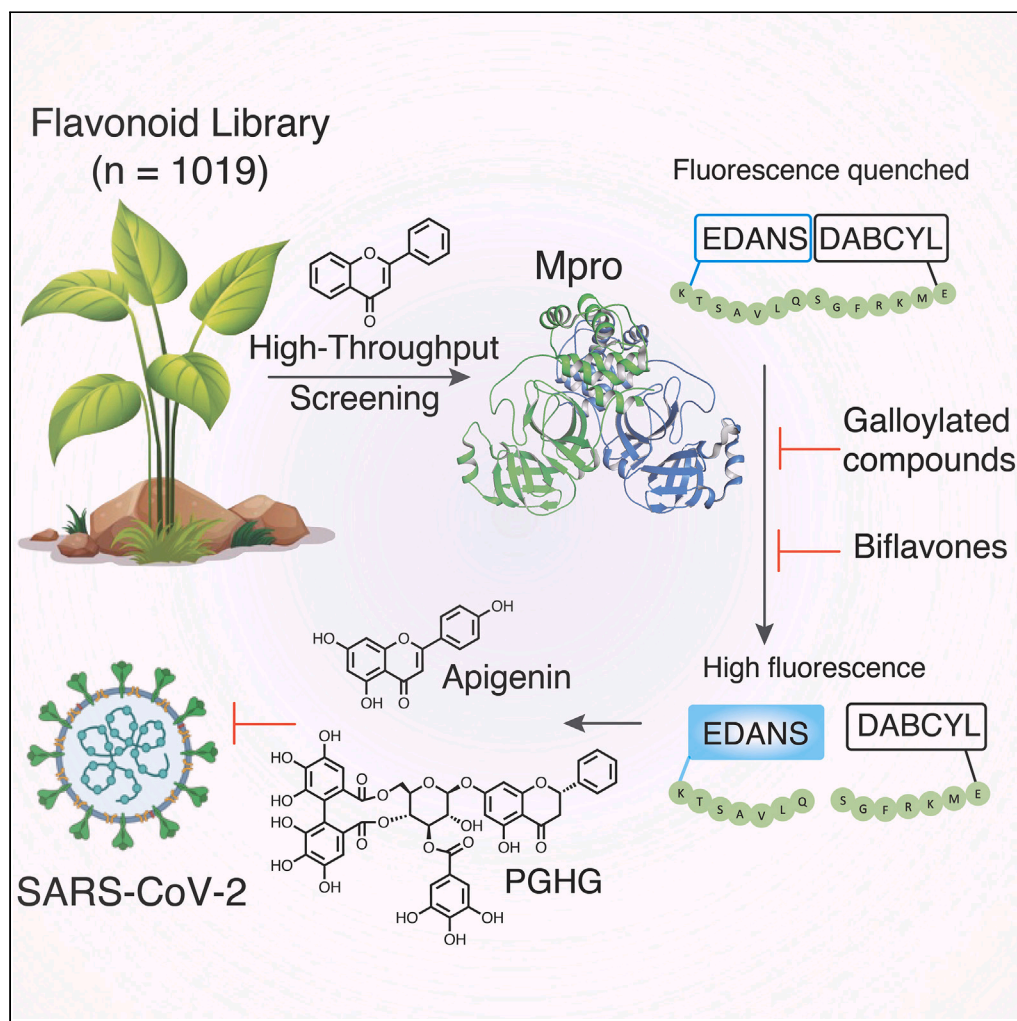


Article

Plant flavonoid inhibition of SARS-CoV-2 main protease and viral replication



Lin Lin, Da-Yuan Chen, Christina Scartelli, ..., Lijun Sun, Mohsan Saeed, Robert Flaumenhaft

rflaumen@bidmc.harvard.edu

Highlights

HTS of a large flavonoid library identified SARS-CoV-2 main protease inhibitors

Galloylated compounds and biflavones were enriched among active compounds

The galloylated pinocembrin, PGHG, occluded the S1 binding site via its galloyl group

PGHG and apigenin were the most potent inhibitors of SARS-CoV-2 replication

Article

Plant flavonoid inhibition of SARS-CoV-2 main protease and viral replication

Lin Lin,^{1,2} Da-Yuan Chen,^{3,4} Christina Scartelli,¹ Huanzhang Xie,² Glenn Merrill-Skoloff,¹ Moua Yang,¹ Lijun Sun,⁵ Mohsan Saeed,^{3,4} and Robert Flaumenhaft^{1,6,*}

SUMMARY

Plant-based flavonoids have been evaluated as inhibitors of β -coronavirus replication and as therapies for COVID-19 on the basis of their safety profile and widespread availability. The SARS-CoV-2 main protease (Mpro) has been implicated as a target for flavonoids *in silico*. Yet no comprehensive *in vitro* testing of flavonoid activity against SARS-CoV-2 Mpro has heretofore been performed. We screened 1,019 diverse flavonoids for their ability to inhibit SARS-CoV-2 Mpro. Multiple structure-activity relationships were identified among active compounds such as enrichment of galloylated flavonoids and biflavones, including multiple biflavone analogs of apigenin. In a cell-based SARS-CoV-2 replication assay, the most potent inhibitors were apigenin and the galloylated pinocembrin analog, pinocembrin 7-O-(3''-galloyl-4'',6''-(5)-hexahydroxydiphenoyl)-beta-D-glucose (PGHG). Molecular dynamic simulations predicted that PGHG occludes the S1 binding site via a galloyl group and induces a conformational change in Mpro. These studies will advance the development of plant-based flavonoids—including widely available natural products—to target β -coronaviruses.

INTRODUCTION

Severe acute respiratory syndrome coronavirus 2 (SARS-CoV-2) is the causative agent of coronavirus disease 2019 (COVID-19), which has killed many millions of people worldwide. Targeted therapies that inhibit viral replication are important additions to the armamentarium to combat not only SARS-CoV-2 but also novel β -coronaviruses that could cause future pandemics. The SARS-CoV-2 main protease (Mpro), also called 3 chymotrypsin-like protease (3CLpro), is required for viral replication and is a validated antiviral target for SARS-CoV-2.^{1–3} This cysteine protease is auto-processed from the viral polyproteins 1a and 1ab and cleaves these polyproteins at 11 sites, releasing non-structural proteins (nsp) that are required for viral replication.⁴ Mpro is highly conserved among β -coronaviruses, particularly around the substrate-binding region,⁵ prompting the development of effective antagonists to this protease, since inhibitors of SARS-CoV-2 Mpro are likely to inhibit Mpro in other β -coronaviruses. Several inhibitors of SARS-CoV-2 Mpro have undergone clinical testing, and nirmatrelvir⁶ and ensitrelvir^{7,8} have received regulatory approval. Ritonavir-boosted nirmatrelvir (Paxlovid) demonstrated excellent efficacy in patients with mild-to-moderate COVID-19 with a high risk of disease progression.^{2,3} Limitations of ritonavir-boosted nirmatrelvir, however, include extensive drug-drug interactions owing to ritonavir,⁹ documented rebound,^{10,11} and modest patient demand.¹² Furthermore, mutations in SARS-CoV-2 Mpro that confer resistance to nirmatrelvir and ensitrelvir have already been identified,¹³ underscoring the importance of developing a variety of Mpro antagonists.

Flavonoids are a family of ~10,000 plant-based compounds whose functions include modulation of enzyme activity, host defense, and providing pigmentation and UV filtration for plants.^{14–16} Flavonoid-enriched extracts are used by traditional medicine practitioners for many indications, including viral illness. Several flavonoids have been shown to have activity against β -coronaviruses in viral replication assays.^{17–19} The possibility that certain flavonoids might inhibit SARS-CoV-2 is attractive since flavonoids can be sourced from abundant agricultural products, are generally orally available, and have a relatively well-studied metabolism.²⁰ Similarly, the safety profile of many types of flavonoids is well established and many flavonoids are commercially available as over-the-counter nutraceuticals.

Soon after the X-ray crystallographic structure of SARS-CoV-2 Mpro was released,²¹ a large number of molecular docking studies were published that predicted high-affinity interactions of several flavonoids within the S1 binding pocket of SARS-CoV-2 Mpro. These studies included those using targeted flavonoid libraries to rank the binding of different compounds²² as well as large libraries of >1 million virtual compounds that included some flavonoids.²³ While potentially useful, such *in silico* screening of small-molecule inhibitors is prone to error.²⁴

¹Division of Hemostasis and Thrombosis, Department of Medicine, Beth Israel Deaconess Medical Center, Harvard Medical School, Boston, MA 02215, USA

²College of Materials and Chemical Engineering, Minjiang University, Fuzhou Institute of Oceanography, Fuzhou, China

³National Emerging Infectious Diseases Laboratories (NEIDL), Boston University, Boston, MA, USA

⁴Department of Biochemistry & Cell Biology, Boston University Chobanian and Avedisian School of Medicine, Boston, MA, USA

⁵Center for Drug Discovery and Translational Research, Department of Surgery, Beth Israel Deaconess Medical Center, Harvard Medical School, Boston, MA 02215, USA

⁶Lead contact

*Correspondence: rflaumen@bidmc.harvard.edu

<https://doi.org/10.1016/j.isci.2023.107602>



In vitro enzyme-based screening programs using a large diverse library of flavonoids have not previously been published. To identify potential flavonoid inhibitors of SARS-CoV-2 Mpro, we performed high-throughput screening of a 1,019 compound flavonoid library using a dequenching-based proteolytic assay.²¹ Compounds that demonstrated inhibition in this fluorescence-based assay were subsequently tested in a mass spectrometry-based label-free assay. Active compounds were then further evaluated in viral replication assays. This systematic campaign identified several flavonoids that inhibited SARS-CoV-2 Mpro as well as viral replication. Moreover, we identified specific flavonoid modifications such as biflavone formation and galloyl group addition that enhanced activity against Mpro. This information will guide future identification and development of flavonoid-based Mpro inhibitors.

RESULTS

Mpro inhibition by flavonoids varies by subclass and flavonoid modification

We screened a large collection of flavonoids ($n = 1,019$) using an EDANS/Dabcyl-based fluorescence dequenching assay to evaluate the ability of purified Mpro to cleave a peptide substrate (KTSAVLQSGFRKM) containing the nsp4/nsp5 cleavage site, naturally targeted by the protease.²⁵ When converted into a high-throughput format, the assay showed a Z score of 0.74. The flavonoid library included all the major subclasses of flavonoids including flavones, flavonols, flavanones, flavanonols, flavans, isoflavonoids, and anthocyanidins (Figure 1A). We screened the flavonoid collection in duplicate at a concentration of 17 μM and plotted activity as percent DMSO controls on each plate (Figure 1B). This analysis demonstrated good correlation of duplicates ($r = 0.71$). Values from the DMSO control wells demonstrated a CV of 6.3. Subclass analysis demonstrated active compounds among all subclasses except flavanonols and anthocyanidins (Figure 1C). Evaluation of Mpro inhibition among all compounds demonstrated an inflection point at 50 compounds (Figure S1). However, 36 of these compounds failed to demonstrate adequate dose curves upon retesting owing either to high background fluorescence or interference with EDANS fluorescence. The remaining compounds were evaluated to determine their half-maximal inhibitory concentration (IC_{50}) for inhibition of Mpro. This analysis identified 9 compounds with an $\text{IC}_{50} < 50 \mu\text{M}$ (Figure 1D). These active compounds included all subclasses except flavanonols, anthocyanidins, and isoflavonoids.

Screening a library of compounds with a common backbone facilitates identification of features that promote activity. We evaluated several characteristics to determine whether or not they were enriched in our active compounds. Comparison of the molecular weights of active flavonoids compared with non-active flavonoids showed that active flavonoids had substantially higher molecular weights (639.01 vs. 432.02, $p < 0.0001$). A wide variety of enzymatic pathways in plants introduce modifications onto the skeletal structure of flavonoids.²⁶ Typical modifications of high-molecular-weight flavonoids included glycosylation, prenylation, biflavone formation, and galloylation.²⁷ Biflavone formation was significantly increased in active compounds compared to inactive compounds (44% vs. 6.1%, $p = 0.001$, Fisher Exact Test; Figure 1E). Similarly, galloylation was increased in active flavonoids compared to inactive flavonoids (33% vs. 2.2%, $p < 0.001$, Fisher Exact Test; Figure 1F). In contrast, prenylation was not significantly increased in active compounds compared to inactive compounds (22% vs. 18%, $p = \text{NS}$). These analyses indicate that flavonoids modified by biflavone formation or galloylation are enriched in the group of flavonoid compounds that inhibit Mpro.

To discover lead flavonoid Mpro inhibitors, we further evaluated the most potent flavonoid Mpro inhibitors. Four compounds with IC_{50} values of 5–15 μM were identified, including amentoflavone, 3,8'-biapigenin, pinocembrin 7-O-(3''-galloyl-4''-6''-(S)-hexahydroxydiphenoyl)-beta-D-glucose (PGHG; compound identifier (CID) 129896874), and jaceidin triacetate. To confirm the protease-inhibiting potential of these compounds, they were further evaluated in a label-free assay. Specifically, we quantified the cleavage of the substrate by mass spectrometry, monitoring the loss of full-length substrate and production of cleavage products (Figure S2A). This assay demonstrated that amentoflavone, 3,8'-biapigenin, PGHG, and jaceidin triacetate completely inhibited the Mpro activity (Figure S2B).

Biflavones of apigenin inhibit Mpro

The presence of several analogs of biflavones involving apigenin in the library enabled evaluation of structure-activity relationships (SARs) among this family of compounds. Amentoflavone and 3,8'-biapigenin (Figure 2A) were identified in the initial screen. A substitution of a methoxy (OMe) group for the hydroxyl (OH) group at the 4''' position was not well tolerated, resulting in higher IC_{50} values of isoginkgetin and podocarpus flavone A (Figure 2B). Loss of the 2–3 double bond pair in 2,3-dihydroheaveaflavone and tetrahydroamentoflavone, converting the flavone into a flavanone, also resulted in substantial loss of activity (Figure 2B). In contrast, analogs such as bilobetin and ginkgetin showed Mpro inhibitory activity comparable to amentoflavone and 3,8'-biapigenin (Figure 2B), extending the number of biflavones capable of inhibiting Mpro.

Given the extensive SAR the library provided for amentoflavone analogs, we performed a docking study (Autodock Vina)²⁸ to model the interactions between amentoflavone and the catalytic domain of Mpro utilizing the reported high-resolution crystal structure of Mpro (PDB Code: 7B3E).²⁹ The top binding pose (ΔE : 8.5 kcal/mol) from the simulation indicated that amentoflavone was able to occupy the substrate-binding site of Mpro to inhibit its enzymatic activity (Figure 2C). The formation of multiple hydrogen bonds (H-bonds) between the inhibitor and protein contributed to the stabilization of the structural complex (Figure 2D). Notably, the OH group at the 7'' position formed an H-bond with the main-chain NH of Gly143 (2.39 Å) and a side-chain SH (3.58 Å) of Cys145. Gly143 and Cys145, together with Ser144, constitute the "oxyanion hole" of this cysteine protease and perform a pivotal role in catalyzing the hydrolysis of protein substrate. Moreover, H-bond interactions could be observed between the 7-OH and main-chain carbonyl (C=O) (2.30 Å) of Glu166, as well as between 4''-OH and main-chain NH (2.04 Å) or C=O (2.57 Å) of Thr26. Additional inhibitor-protein interactions that also contributed to the stabilization of the structural complex include $\text{NH}_2-\pi$ interaction with Gln189 and hydrophobic interactions with Met49 and Met165. Furthermore, the binding interactions

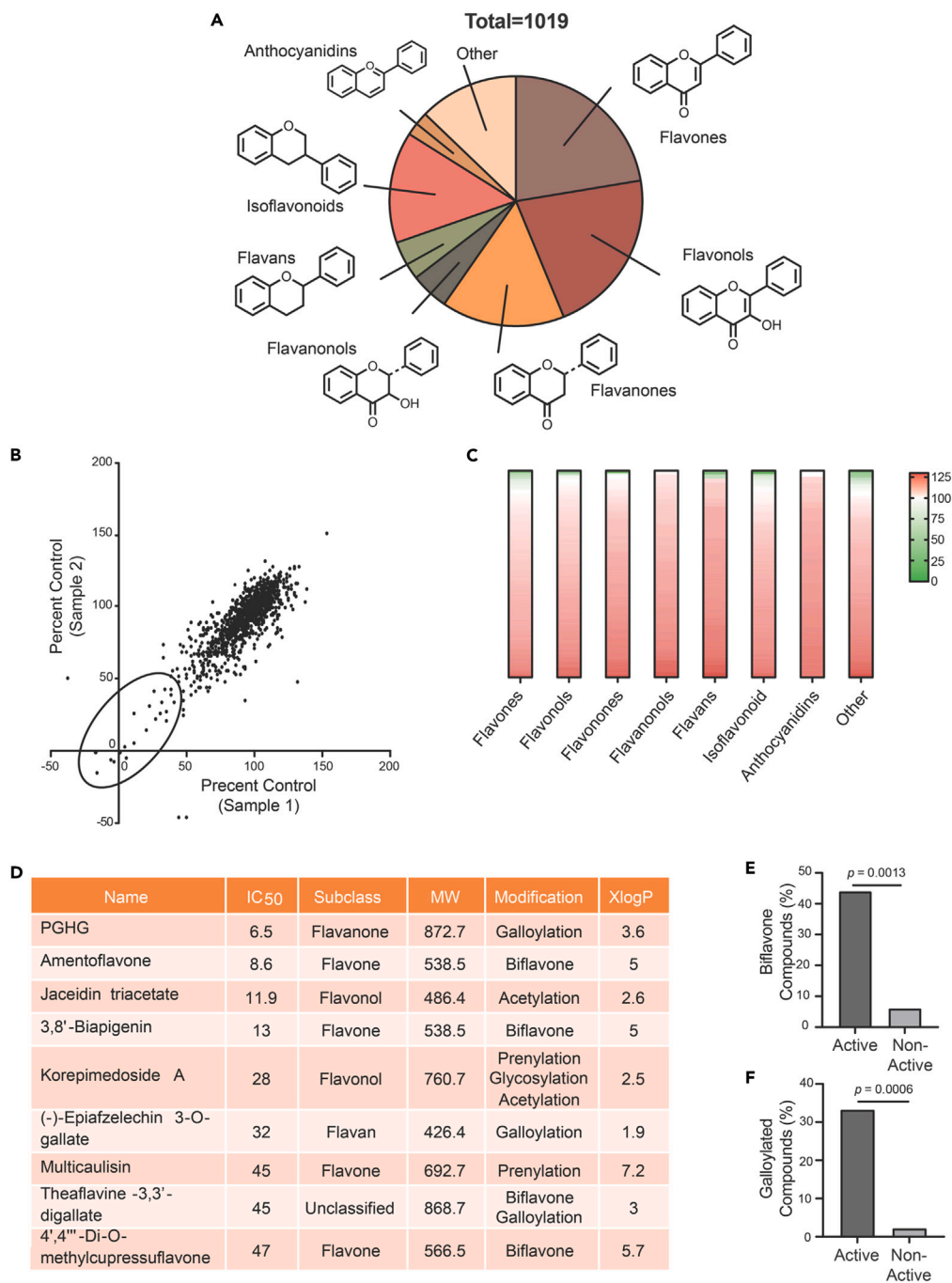


Figure 1. Identification of novel flavonoid inhibitors of the SARS-CoV-2 Mpro

(A) Distribution of flavonoids among the different flavonoid subclasses in the small molecule library.

(B) Inhibitory activity of flavonoids evaluated at 17 μ M in duplicate (sample 1 vs. sample 2) in the SARS-CoV-2 Mpro fluorescence-based enzymatic assay. Encircled compounds inhibit Mpro to <50% of baseline activity.

(C) Heatmap demonstrating the distribution of active (green) and inactive (white and red) compounds among the indicated flavonoid subclasses. Key in upper right corner of panel represents the fluorescence value (RFU) of duplicate samples (green indicates inhibition of Mpro activity, white and red indicate no inhibition).

(D–F) Characteristics of verified flavonoid inhibitors of SARS-CoV-2 Mpro. Compared to flavonoids within the entire library, active compounds were significantly enriched in (E) biflavones and (F) galloylated compounds.

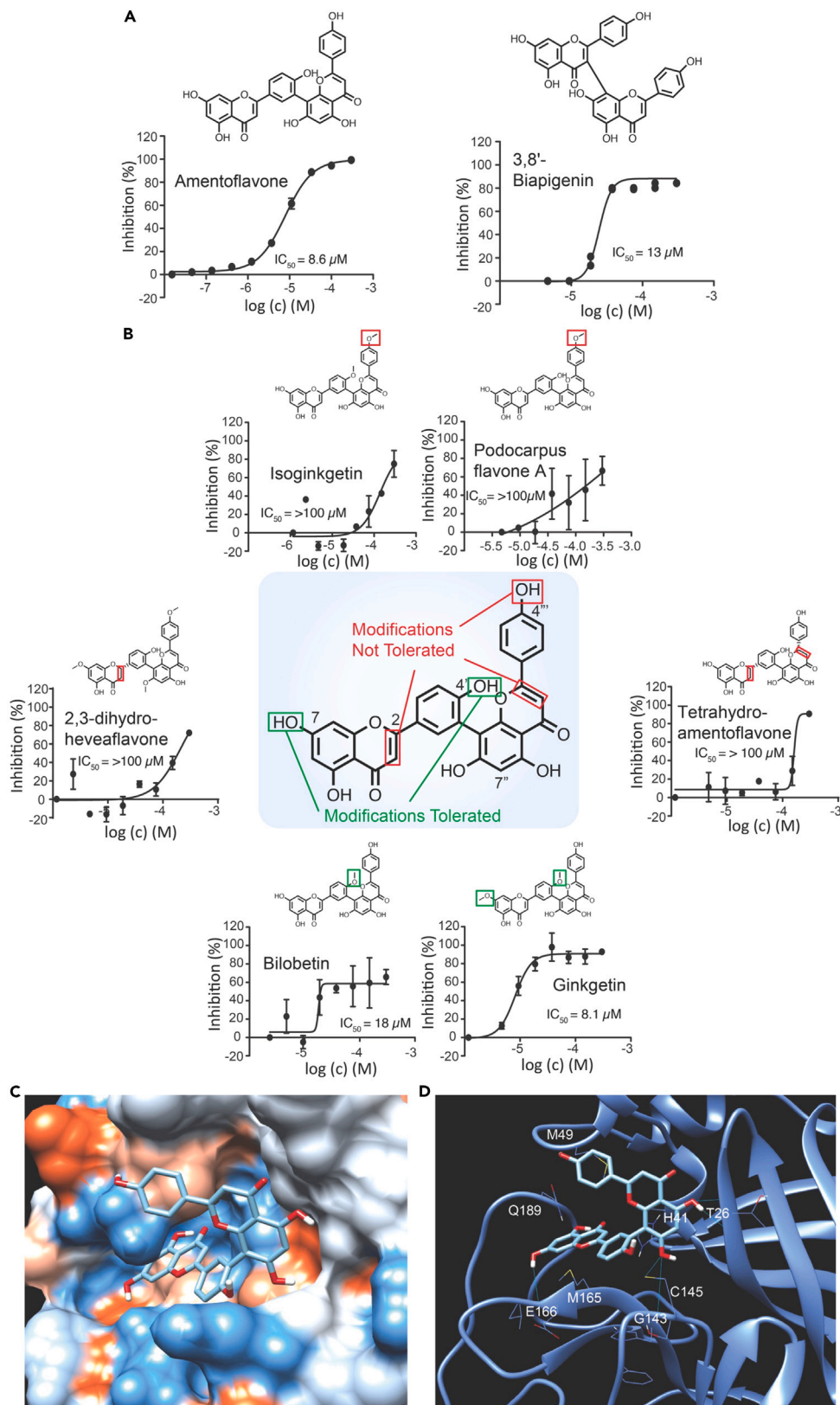


Figure 2. Evaluation of apigenin biflavones as inhibitors of SARS-CoV-2 Mpro

(A) Comparison of IC₅₀s of amentoflavone and 3,8'-biapigenin as inhibitors of Mpro.

(B) Structure-activity relationships of amentoflavone inhibition of Mpro activity. Features highlighted in red indicate essential elements of amentoflavone inhibition of Mpro. Hydroxyl groups indicated in green can be substituted without impairing activity of the biflavone.

(C) The binding pose of amentoflavone (structure shown as sticks; red: oxygen; blue: carbon) in the catalytic domain of Mpro (shown as surface; red: hydrophilic; blue: hydrophobic).

(D) H-bond interactions (shown as blue dashed line) between amentoflavone (structure shown in cyan as sticks) and Mpro (backbone shown in blue as ribbon/helix/coil, and side chain shown as wire; red: oxygen; blue: carbon, yellow: sulfur).

revealed by the docking simulation might shed light on the experimental SAR in this class of biflavones. For instance, the 4'-OH and the 4'''-OH of amentoflavone were positioned toward a hydrophobic and hydrophilic pocket, respectively. Therefore, substitution of the 4'-OH with a hydrophobic OMe (e.g., Ginkgetin) was better tolerated than that of the 4'''-OH. It is also conceivable that the 2,3- (as well as the 2'',3''-) double bond of amentoflavone serves a determinative role to orientate the two flavone fragments for maximal binding with Mpro. Reducing either double bond (e.g., 2,3-dihydroveveaflavone) would dramatically alter the three-dimensional structure, leading to impairment of its binding to Mpro and reduced inhibitory activity.

Amentoflavone (3',8''-biapigenin) and 3,8'-biapigenin are formed from conjugation of two apigenin molecules. Follow-up assays confirmed the ability of apigenin to inhibit Mpro with an IC₅₀ of 20 ± 9 μM. Evaluation of apigenin analogs revealed a few compounds with moderate inhibition against Mpro (Figure S3). Several other apigenin analogs showed little to no activity against Mpro. While the apigenin SAR provided validation of apigenin as an inhibitor of Mpro, it was not sufficiently detailed to enable accurate modeling using molecular docking.

PGHG inhibits Mpro

High-throughput screening with mass spectrometry confirmation also identified PGHG and jaceidin triacetate as inhibitors of SARS-CoV-2 Mpro. Both compounds showed inhibitory activity that was comparable to or better than the previously described Mpro inhibitors baicalein and myricetin and apigenin and its analogs (Figure 3A). In contrast to PGHG, pinocembrin itself showed relatively poor inhibition of Mpro (Figure S4). Jaceidin triacetate was found to be toxic in Vero E6 cells at concentrations that inhibited Mpro and was not pursued further. Baicalein and myricetin showed inhibition in the initial screen at 17 μM but did not make the original cutoff for further analysis.

Mpro can be blocked either by irreversible inhibitors that covalently bind the active site Cys145 or by reversible inhibitors that occlude the S1 binding pocket. High-resolution structures from crystals of baicalein (PDB: 6M2N) and myricetin (PDB: 7B3E) in complex with SARS-CoV-2 Mpro demonstrate very different orientations of these flavonoids in the S1 binding pocket of Mpro despite their substantial structural similarity. Myricetin in complex with Mpro is predicted to become covalently bound to the active cysteine Cys145 at the 2' position.²⁹ In contrast, baicalein associates with Mpro non-covalently through hydrogen bonding with main chains of Leu141, Gly143, and Ser144, as well as the side chains of Asn142,³⁰ thereby shielding access to the C145 active site. To assess whether PGHG, apigenin, amentoflavone, and 3,8'-biapigenin bind reversibly or irreversibly, we performed jump dilution reversibility assays. These studies showed that inhibition of myricetin was resistant to dilution, indicating an irreversible mechanism of binding, consistent with the crystal structure indicating a covalent interaction with Cys145 (Figure 3B). In contrast, inhibition of Mpro by baicalein, apigenin, amentoflavone, and PGHG was completely reversed by dilution, indicating a reversible mechanism of inhibition (Figure 3B).

To better understand the mechanism by which PGHG reversibly inhibits Mpro activity, we performed docking studies. In initial studies, the top binding pose (ΔE : 10.9 kcal/mol) showed that PGHG was able to occupy the substrate-binding site of Mpro. However, this pose did not take into account the action of solvents, resulting in complete exposure of a hydrophobic phenyl to water (Figure S5A). To obtain a more accurate and stable structure of the Mpro-PGHG complex, we performed all-atom, explicit water molecular dynamics (MD) simulations. During the 200 ns simulation, although the conformation of the macrocyclic part of PGHG remained relatively stable, the flavonoid side chain changed substantially. In the first 85 ns of the simulation, the flavonoid moiety spontaneously adjusted, sliding toward a relatively hydrophobic region formed by Pro168, Leu167, and Ala191 (Figure 4A). The change in position of the flavonoid induced a conformation change of Mpro. In the subsequent 120 ns of the simulation, the conformation of PGHG and Mpro remained relatively stable, indicating that the structure had converged. The highest root-mean-square deviation (RMSD) value reached 3.91 Å at ~85 ns, during which time Mpro and PGHG induced conformational changes in the complex. The system then stabilized, with most of RMSD values less than 3 (Figure 4B), indicating that the system achieved equilibrium within the simulation time and that the force field and simulation protocols are adequate. Root-mean-square fluctuation (RMSF) values of Mpro complexed with PGHG indicated the flexibility of each amino acid residues in the protein (Figure 4C).

Analysis of the all-atom MD simulation demonstrated electrostatic interactions of the PGHG with components of the Mpro binding pocket including the catalytic diad. The binding energy (ΔG_{total}) of PGHG with Mpro calculated using the molecular mechanics Poisson-Boltzmann surface area (MM-PBSA) method was -58.64 ± 3.17 (Table 1). The contributions to the binding free energy from the von der Waals (vdw) and electrostatic interactions were $\Delta E_{\text{vdw}} = -72.12 \pm 0.47$ and $\Delta E_{\text{ele}} = -54.47 \pm 2.99$, respectively. The polar and nonpolar solvation energy contributions to ΔG_{solv} were $\Delta E_{\text{polar}} = 76.43 \pm 0.94$ and $\Delta E_{\text{nonpolar}} = -8.49 \pm 0.15$, respectively. These calculations indicate that Mpro-PGHG binding is largely governed by electrostatic interactions rather than polar interactions. Energy composition analysis invoked several interactions between PGHG and residues involved in the proteolytic activity of Mpro. PGHG is predicted to interact with His41 ($\Delta G_{\text{total}} = -5.34$) and Cys145 ($\Delta G_{\text{total}} = -1.15$), which form the catalytic diad of this cysteine protease. Glu166 ($\Delta G_{\text{total}} = -3.54$) functions in substrate recognition.

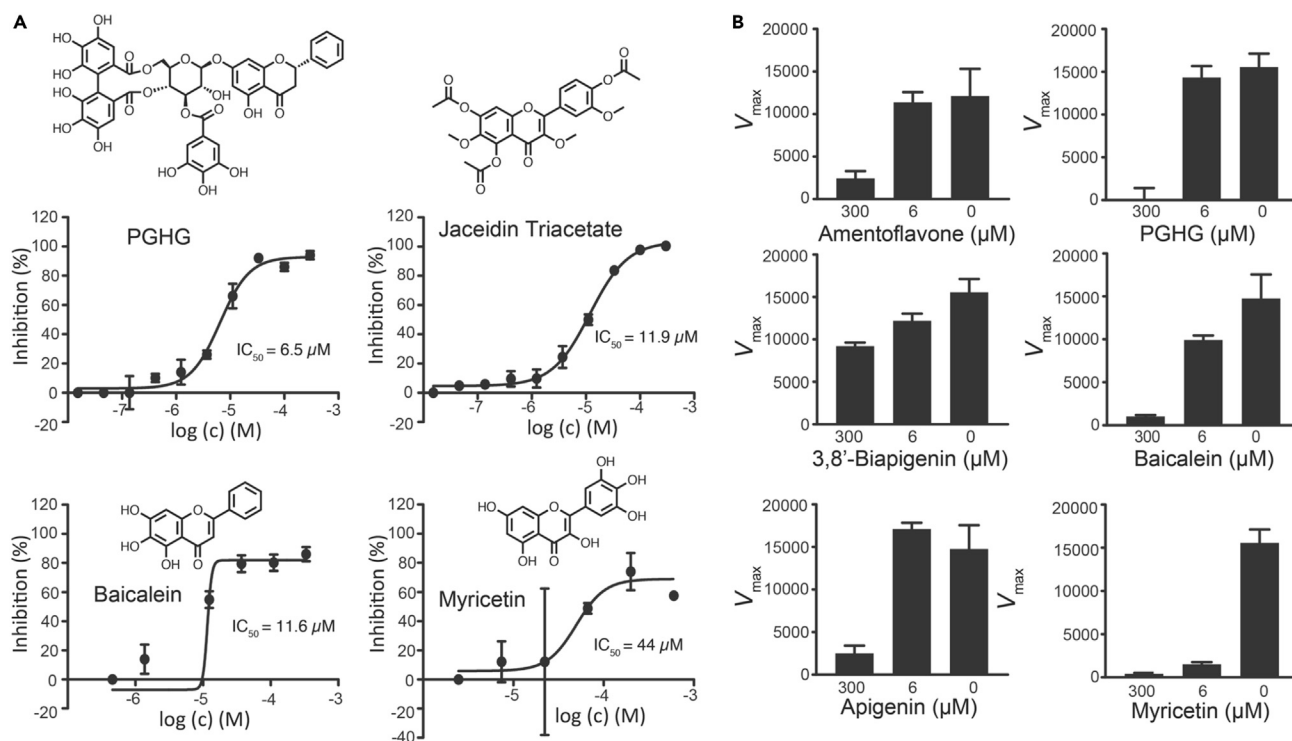


Figure 3. Reversible and irreversible inhibitors of SARS-CoV-2 Mpro

(A and B) Comparison of IC₅₀s of (A) PGHG, jaceidin triacetate, baicalein, and myricetin. (B) Evaluation of reversibility of amentoflavone, PGHG, 3,8'-biapigenin, baicalein, apigenin, and myricetin.

Additionally, PGHG interacts with Met49, Pro168, Gln189, Cys44, Met165, Leu167, Tyr54, Val42, and Thr190 in Mpro (Table 2). The interactions of different moieties of PGHG with residues within the substrate-binding pocket of Mpro are shown in Figures 4D and S5B. This pose invokes the 3'-galloyl group in interactions with Cys145, Gly143, and Ans142 and is associated with an ester in PGHG that interacts with His41. These results indicate an essential role for hydrogen bonding via hydroxyl groups of the galloyl moiety in the action of PGHG.

Evaluation of Mpro inhibitors in a SARS-CoV-2 replication assay

Inhibition of Mpro does not reliably predict the ability of a compound to inhibit SARS-CoV-2 replication. A compound may be unable to enter cells, extruded from or rapidly metabolized by the cells, or bind more abundant proteins nonspecifically. To assess which of the flavonoid Mpro inhibitors block SARS-CoV-2 replication, flavonoids were tested in a Vero E6-based SARS-CoV-2 replication assay that relies on immunofluorescence microscopy to detect infected cells by staining for the viral nucleocapsid (N) protein. Evaluation of baicalein, myricetin, apigenin, amentoflavone, 3,8'-biapigenin, and PGHG demonstrated different activities of each of the compounds (Figure 5A). Consistent with the published literature, baicalein inhibited SARS-CoV-2 infection, although it was not as effective in this assay as previously reported³¹ Myricetin, with no known activity against SARS-CoV-2,²⁹ was only inhibitory at 100 μM. Apigenin showed activity that was slightly better than baicalein at 50 μM (Figures 5A and 5B), whereas the biflavones showed little, if any, activity. The most potent flavonoid inhibitor of SARS-CoV-2 was PGHG (Figure 5C). Dose-response analysis revealed an IC₅₀ of 4.9 μM, and no cytotoxicity was seen at this concentration in Vero E6 cells (Figure 5C). Toxicity was observed, however, with a half-maximal cytotoxicity concentration (CC₅₀) of 15.6 μM, resulting in a selectivity index of 3.2 in the Vero E6 cells. For initial toxicity testing, we evaluated PGHG in a mouse model of endotoxemia-induced sepsis since PGHG could be used in the setting of systemic illness and testing PGHG toxicities in sepsis may be more sensitive than testing only in healthy mice. Evaluation of PGHG toxicity following intraperitoneal injection of lipopolysaccharide (LPS)-induced sepsis showed that 5 μg/g PGHG did not significantly affect the progression of sepsis as monitored using a standardized score (Figure S6).

DISCUSSION

We performed a comprehensive *in vitro* screen of a large library of flavonoids in order to identify inhibitors of SARS-CoV-2 Mpro. While there have been many *in silico* studies that have demonstrated potential interactions with Mpro and some *in vitro* studies using small collections of flavonoids,³² our study is unique in providing a large-scale evaluation of multiple flavonoid classes in an enzymatic assay, providing extensive information about SARs. The effort both demonstrated certain flavonoid modifications that contribute to Mpro inhibition and identified novel flavonoid inhibitors of SARS-CoV-2 replication.

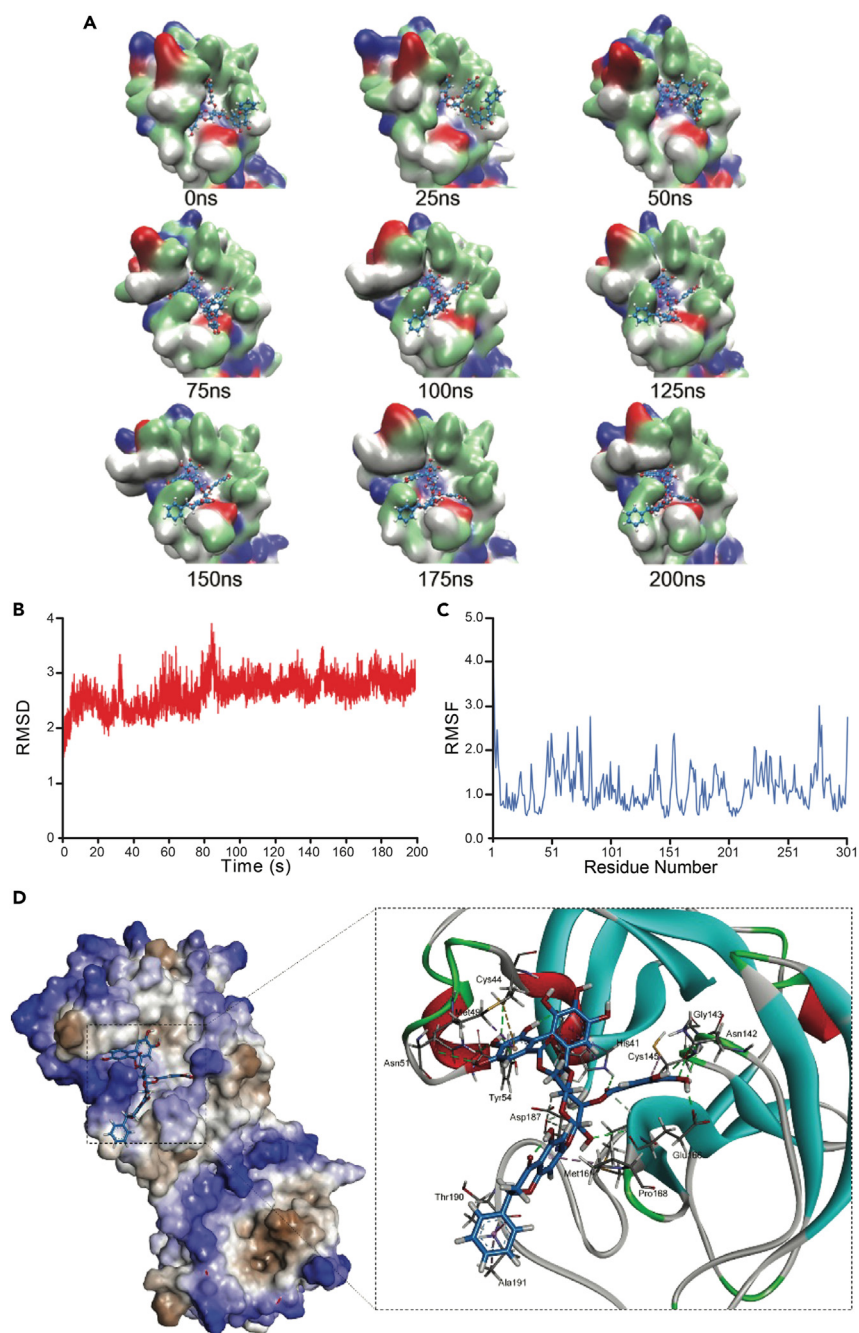


Figure 4. Molecular dynamic simulation of PGHG binding to SARS-CoV-2 Mpro

(A) Snapshots are shown of the PGHG-Mpro complex at the indicated simulation times. The Mpro is colored by residue type (acidic: red, basic: blue, polar: green, nonpolar: gray), while PGHG is shown in sapphire.

(B) RMSD fluctuation of Mpro in complex with PGHG.

(C) RMSF fluctuation of Mpro in complex with PGHG.

(D) The predicted binding of PGHG (depicted as sapphire sticks) within the S1 binding pocket of Mpro is shown. The surrounding residues in the Mpro binding pocket are depicted as gray sticks.

We found that both biflavone formation and galloylation are flavonoid modifications that promote inhibition of SARS-CoV-2 Mpro. Biflavones were enriched among active compounds, and these active biflavones have a significantly higher average molecular mass than that of the entire library (628.05 vs. 432.02, $p < 0.001$). Their increased size may enable biflavones to more effectively occlude the S1 binding pocket of Mpro compared to smaller flavonoids. The average molecular mass of active galloylated flavonoids was also large compared to that of the

Table 1. Average binding energy and its components obtained from the MM-GBSA calculation for the complex of Mpro-PGHG.

Contribution	Energy (kcal/mol)
ΔE_{vdw}	-72.12 ± 0.47
ΔE_{ele}	-54.47 ± 2.99
ΔE_{polar}	76.43 ± 0.94
$\Delta E_{nonpolar}$	-8.49 ± 0.15
ΔG_{gas}	-126.58 ± 3.03
ΔG_{solv}	67.94 ± 0.95
ΔG_{total}	-58.64 ± 3.17

entire library (722.6 vs. 432.3, $p < 0.001$). Of note, the structure of baicalein in complex with SARS-CoV-2 Mpro (PDB: 6M2N) demonstrates hydrogen bonding between the 6,7,8-hydroxyl groups and G143/L141 and side chains of Ser144/His163, thereby shielding the C145 active site.³³ Myricetin also contains three hydroxyl groups in series at 3',4',5' positions that form H-bonds within the S1 pocket of Mpro, orienting myricetin in the opposite direction as baicalein.²⁹ However, in the case of myricetin, there is a nucleophilic attack of Cys145 resulting in covalent bond formation at the 2' position. Whether the three phenolic hydroxyl groups that characterize inhibitory galloylated flavonoids—such as PGHG, (–)-epiafzelechin 3-O-gallate, and theaflavine-3,3'-digallate—orient similarly to inhibit Mpro activity remains to be proven definitively. Nonetheless, our MD simulations suggest shielding of the catalytic diad by the galloyl group (Figure 4D). This phenomenon could explain the enrichment of flavonoids containing galloyl groups among Mpro inhibitors (Figure 1F).

Among flavonoids containing galloyl groups, PGHG was evaluated in more detail since it was the most potent galloylated flavonoid with regard to Mpro antagonism and SARS-CoV-2 inhibition. This compound is an ellagitannin composed of pinocembrin, hexahydroxydiphenic acid, and gallic acid linked to glucose.^{34,35} It is found in the aerial part of *Penthorum chinense* pursh, which is widely distributed in eastern Asia and is used in China as a dietotherapy for liver disease as well as other indications.^{35,36} In our studies, PGHG had relatively low autofluorescence, enabling its identification in a fluorescence-based enzymatic assay in which it demonstrated an IC_{50} for Mpro in the low micromolar range (Figure 3). It showed significant inhibition of SARS-CoV-2 replication in the Vero E6-based assay (Figure 5), with an IC_{50} in the viral replication assay of 4.9 μM , very close to its IC_{50} for inhibition of Mpro (Figures 3 and 5). However, toxicity was observed in Vero E6 cells with a CC_{50} of 15.6 μM (selectivity index of 3.2). Limited *in vivo* testing showed that 5 $\mu g/g$ PGHG did not worsen the progression of LPS-induced sepsis compared to vehicle in mice following infusion of LPS (Figure S6). A small difference in sepsis score is observed 30 m after injection of PGHG; however, this difference is short-lived. Additionally, PGHG appears to be tolerated in healthy mice at 25 $\mu g/g$. Nonetheless, formal dose-ranging toxicity and toxicokinetic studies evaluating organ level effects of PGHG and studies comparing the efficacy of PGHG with its toxicity in an animal model of SARS-CoV-2 infection will be required to determine whether or not PGHG has a suitable therapeutic window. Clinically, there is substantial experience with human ingestion of chinense pursh extract, but little is known about the clinical effects of purified PGHG consumption in humans.

In contrast to PGHG, apigenin is an extremely common flavonoid, considered among the five most ubiquitous flavonoids in the plant kingdom.^{37,38} It is particularly abundant in commonly consumed foods such as celery, parsley, and chamomile.^{38,39} Inexpensive purified preparations of apigenin (98% pure) are readily available. In an enzymatic assay, apigenin was a less potent inhibitor of Mpro than its biflavones, amentoflavone, 3,8'-biapigenin, bilobetin, and ginkgetin. Docking studies of amentoflavone informed by extensive SAR of the apigenin

Table 2. Energy decomposition

Residue	ΔE_{vdw}	ΔE_{ele}	ΔG_{sol}	ΔG_{total}
HIS41	-4.2308	-3.2889	2.5181	-5.3408
GLU166	-2.3126	-14.3267	13.4835	-3.5427
MET49	-3.0940	-1.4066	1.6570	-3.2872
PRO168	-1.9049	-0.4623	0.5939	-2.1764
GLN189	-3.7629	-2.3084	4.6622	-2.1381
CYS44	-1.0076	-2.8682	2.1298	-1.8340
MET165	-2.2744	-0.3674	1.0370	-1.7453
LEU167	-1.6281	-0.9683	1.1249	-1.5776
TYR54	-0.8209	-0.8074	0.4029	-1.2927
VAL42	-1.2632	-0.3888	0.5365	-1.1532
CYS145	-1.0537	-0.6670	0.6590	-1.1515
THR190	-1.2631	-0.0178	0.4080	-1.0228

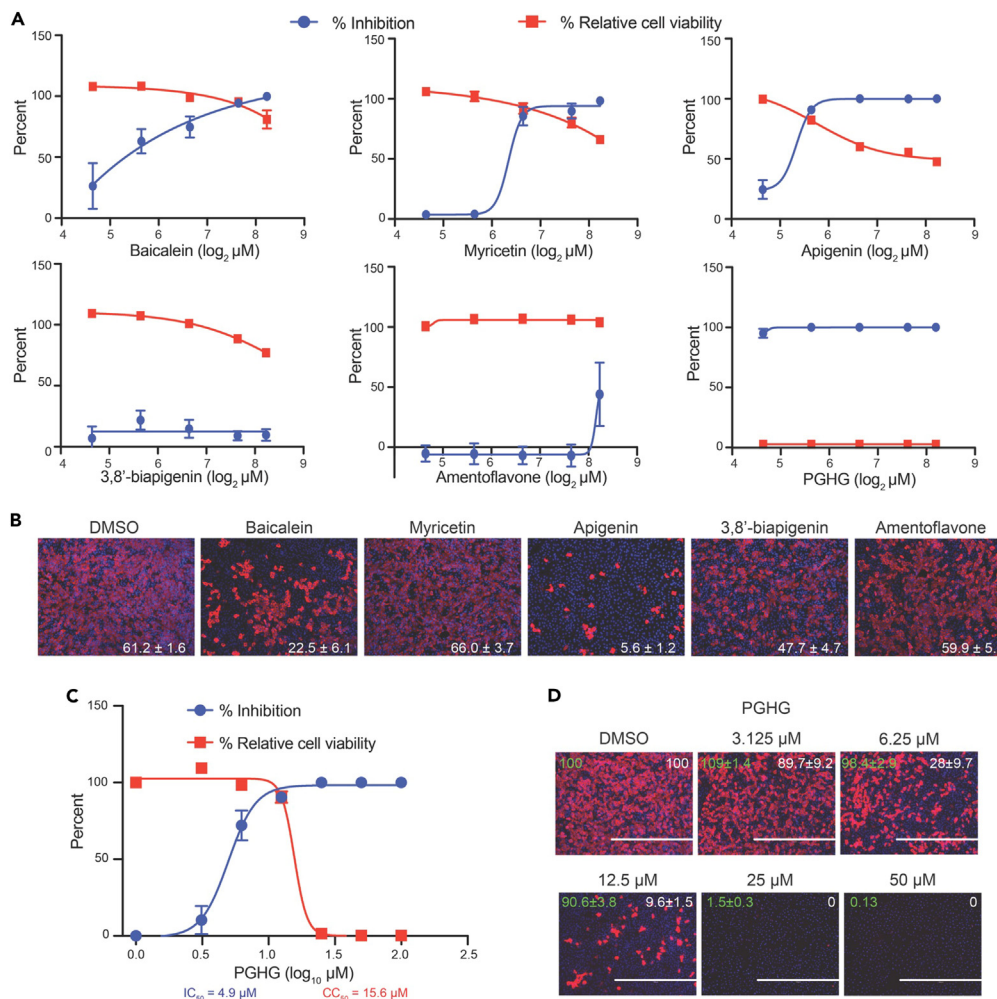


Figure 5. Inhibition of SARS-CoV-2 replication by flavonoids

(A) Dose curve of inhibition of SARS-CoV-2 replication in Vero E6 cells by baicalein, myricetin, apigenin, 3,8'-biapigenin, amentoflavone, and PGHG.

(B) Images of inhibition of viral replication by baicalein, myricetin, apigenin, 3,8'-biapigenin, and amentoflavone compared with DMSO control. Percent of monolayer stained with anti-SARS-CoV nucleocapsid antibody is indicated in the lower right-hand corner.

(C) Activity of PGHG in the SARS-CoV-2 replication assay.

(D) Images of viral replication by increasing concentration of PGHG. Percent of viral infection (average ±SD; green) and cell viability (average ±SD; white) indicated in the upper corners of the image. The scale bar represents 750 μm.

biflavones suggested that it bound to Mpro by forming some of the key binding interactions as observed in the cocrystal structures of Mpro in complex with baicalein or myricetin, including H-bonds with Gly143 and Cys145 in the “oxyanion hole” of the catalytic reaction site in the cysteine protease. However, the biflavones had little activity in the SARS-CoV-2 viral replication assay. Thus, while amentoflavone is also widely available as an over-the-counter nutraceutical, it does not appear to hold promise for COVID-19 therapy. Apigenin is more promising in this regard. While it shows some toxicity in cell culture, it inhibits viral replication at concentrations that are not toxic (Figure 5). These findings are consistent with those of Chaves et al., who found that apigenin inhibits SARS-CoV-2 replication with an IC₅₀ of 5.11 ± 0.26 and was tolerated by Calu-3 cells with a CC₅₀ of 302 ± 15.⁴⁰ Whether or not apigenin affects SARS-CoV-2 replication or the course of infection in animal models has not yet been evaluated.

Baicalein and myricetin have previously been identified as inhibitors of Mpro. Baicalein was identified in an evaluation of a Shuanghuan-glian preparation for the ability to inhibit Mpro.³³ It was also found to inhibit SARS-CoV-2 replication. Determination of baicalein’s mechanism of action in blocking SARS-CoV-2 replication indicated that, in addition to inhibiting Mpro, it interferes with oxidative phosphorylation in a manner dependent on the mitochondrial permeability pore.⁴¹ Although our studies indicate less potent IC₅₀s in both Mpro inhibition and viral replication assays, perhaps owing to differences in techniques, the results are largely consistent. Baicalein is currently the only flavonoid Mpro inhibitor that has been tested *in vivo* for anti-SARS-CoV-2 effect.⁴² Using a human ACE2 transgenic mouse model, Song et al. showed that 50–200 μg/g of the crystal form β of baicalein prevented reduction in body weight and decreased lung injury resulting from SARS-CoV-2

infection.⁴² Myricetin was initially identified in a virtual screen of 8,700 compounds for inhibitors of Mpro. It was subsequently shown to inhibit Mpro in an enzymatic assay. X-ray crystal structure in complex with Mpro indicated covalent binding to Cys145.⁴² Although this study did not find inhibition of SARS-CoV-2 replication by myricetin, we find that myricetin inhibits SARS-CoV-2 replication under the conditions of our assay (Figure 5), albeit less potently than PGHG, baicalein, or apigenin.

Limitations of study

While these results raise the possibility that flavonoids could be developed as safe and effective targeted therapies for COVID-19, several limitations of these studies need to be considered. Intrinsic fluorescence and quenching by many flavonoids in our library precluded their evaluation in a fluorescence-based enzymatic assay. By focusing on flavonoids with little intrinsic fluorescence at $\lambda_{\text{abs}} = 336 \text{ nm}$ and $\lambda_{\text{em}} = 490 \text{ nm}$, we may have missed flavonoids that effectively inhibit Mpro. Inhibition of native Mpro in the context of SARS-CoV-2 viral replication is meaningfully different from inhibition of cleavage of the Mpro-based peptide used to characterize the inhibitory activity of the flavonoids. The combination of enzymatic and molecular modeling studies provides strong evidence that these compounds interfere with Mpro activity. Yet many flavonoids are promiscuous in their activity, and it is possible that they interfere with SARS-CoV-2 replication by additional or alternative activities. The promiscuous nature of flavonoid activity is also a consideration for toxicity, particularly for flavonoids whose purified forms have not been extensively evaluated in humans, such as PGHG. Although initial testing showed that PGHG did not promote the progression of sepsis in a murine endotoxemia model (Figure S6), dose-finding studies in an animal model of SARS-CoV-2 infection will be required to thoroughly assess toxicity.

Despite these limitations, screening of a large library of flavonoids that includes representation of all flavonoid subclasses and a wide range of flavonoid modifications provides a comprehensive evaluation of flavonoid-Mpro interactions. Such interactions can be missed by *in silico* docking studies performed in the absence of any guiding SARs, which are prone to error.²⁴ There was only marginal overlap between our enzymatic screening of flavonoid Mpro inhibitors and previous *in silico* screens.²² Conversely, screens of small collections of flavonoids^{43,44} or extracts of natural products^{45,46} are far less inclusive and lack the extensive opportunity for SARs provided by enzymatic screening of a large flavonoid library. The finding that biflavones and galloylated flavonoids are enriched in Mpro inhibitors could help guide future identification and development of flavonoid-based treatments for COVID-19.

STAR★METHODS

Detailed methods are provided in the online version of this paper and include the following:

- KEY RESOURCES TABLE
- RESOURCE AVAILABILITY
 - Lead contact
 - Materials availability
 - Data and code availability
- EXPERIMENTAL MODEL AND STUDY PARTICIPANT DETAILS
 - Biocontainment
- METHOD DETAILS
 - Mpro expression and purification
 - High-throughput screening of the flavonoid library
 - Mpro activity assays
 - Immunofluorescence of SARS-CoV-2 viral replication
 - Molecular docking
 - Molecular dynamics simulation
 - Endotoxemia Model
- QUANTIFICATION AND STATISTICAL ANALYSIS

SUPPLEMENTAL INFORMATION

Supplemental information can be found online at <https://doi.org/10.1016/j.isci.2023.107602>.

ACKNOWLEDGMENTS

The authors would like to thank Jennifer Smith, Ph.D., and other faculty of the Institute for Chemistry and Cell Biology at Harvard Medical School for their invaluable assistance in the acquisition and guidance in the screening of the flavonoid library. This work was supported by the National Institutes of Health grants R35HL135775 (R.F.), U01HL143365 (R.F.), T32HL007917 (M.Y., R.F.), K99HL164888 (M.Y.), the American Society of Hematology Scholar Award (M.Y.), and the Natural Science Foundation of Fujian Province 2021J02052 (L.L.). MS was supported by Boston University Startup Funds and the Foundation for Women's Wellness (FWW).

AUTHOR CONTRIBUTIONS

Conceptualization, R.F.; Methodology, L.L., D.C., H.X., L.S., M.S., G.M.S., and R.F.; Investigation, L.L., D.C., C.S., H.X., G.M.S., and L.S.; Writing – Original Draft, L.L., H.X., L.S., M.S., and R.F.; Writing – Review & Editing, L.L., D.C., H.X., M.Y., M.S., and R.F.; Funding Acquisition, L.L., M.S., and R.F.; Resources, L.L., M.Y., M.S., and R.F.; Supervision, L.L., M.Y., M.S., and R.F.

DECLARATION OF INTERESTS

RF and LL have a patent pending entitled, “Compounds and Methods for Treating Viral Infections”. RF is on the Scientific Advisory Board of NytroPonix and is a founder and consultant at PlateletDiagnostics, LLC.

INCLUSION AND DIVERSITY

One or more of the authors of this paper self-identifies as an underrepresented ethnic minority in their field of research or within their geographical location.

Received: May 11, 2023

Revised: June 15, 2023

Accepted: August 8, 2023

Published: August 10, 2023

REFERENCES

- Zhang, L., Lin, D., Sun, X., Curth, U., Drosten, C., Sauerhering, L., Becker, S., Rox, K., and Hilgenfeld, R. (2020). Crystal structure of SARS-CoV-2 main protease provides a basis for design of improved alpha-ketoamide inhibitors. *Science* 368, 409–412. <https://doi.org/10.1126/science.abb3405>.
- Hammond, J., Leister-Tebbe, H., Gardner, A., Abreu, P., Bao, W., Wisemandle, W., Baniecki, M., Hendrick, V.M., Damle, B., Simón-Campos, A., et al. (2022). Oral Nirmatrelvir for High-Risk, Nonhospitalized Adults with Covid-19. *N. Engl. J. Med.* 386, 1397–1408. <https://doi.org/10.1056/NEJMoa2118542>.
- Arbel, R., Wolff Sagy, Y., Hoshen, M., Battat, E., Lavie, G., Sergienko, R., Friger, M., Waxman, J.G., Dagan, N., Balicer, R., et al. (2022). Nirmatrelvir Use and Severe Covid-19 Outcomes during the Omicron Surge. *N. Engl. J. Med.* 387, 790–798. <https://doi.org/10.1056/NEJMoa2204919>.
- Lee, J., Worrall, L.J., Vuckovic, M., Rosell, F.I., Gentile, F., Ton, A.T., Caveney, N.A., Ban, F., Cherkasov, A., Paetzel, M., and Strynadka, N.C.J. (2020). Crystallographic structure of wild-type SARS-CoV-2 main protease acyl-enzyme intermediate with physiological C-terminal autoprocessing site. *Nat. Commun.* 11, 5877. <https://doi.org/10.1038/s41467-020-19662-4>.
- Zhu, J., Zhang, H., Lin, Q., Lyu, J., Lu, L., Chen, H., Zhang, X., Zhang, Y., and Chen, K. (2022). Progress on SARS-CoV-2 3CLpro Inhibitors: Inspiration from SARS-CoV 3CLpro Peptidomimetics and Small-Molecule Anti-Inflammatory Compounds. *Drug Des. Devel. Ther.* 16, 1067–1082. <https://doi.org/10.2147/dddt.S359009>.
- Owen, D.R., Allerton, C.M.N., Anderson, A.S., Aschenbrenner, L., Avery, M., Berritt, S., Boras, B., Cardin, R.D., Carlo, A., Coffman, K.J., et al. (2021). An oral SARS-CoV-2 M(pro) inhibitor clinical candidate for the treatment of COVID-19. *Science* 374, 1586–1593. <https://doi.org/10.1126/science.abb4784>.
- Mukae, H., Yotsuyanagi, H., Ohmagari, N., Doi, Y., Imamura, T., Sonoyama, T., Fukuhara, T., Ichihashi, G., Sanaki, T., Baba, K., et al. (2022). A Randomized Phase 2/3 Study of Ensitrelvir, a Novel Oral SARS-CoV-2 3C-Like Protease Inhibitor, in Japanese Patients with Mild-to-Moderate COVID-19 or Asymptomatic SARS-CoV-2 Infection: Results of the Phase 2a Part. *Antimicrob. Agents Chemother.* 66, e0069722. <https://doi.org/10.1128/aac.00697-22>.
- Mukae, H., Yotsuyanagi, H., Ohmagari, N., Doi, Y., Sakaguchi, H., Sonoyama, T., Ichihashi, G., Sanaki, T., Baba, K., Tsuge, Y., and Uehara, T. (2023). Efficacy and safety of ensitrelvir in patients with mild-to-moderate COVID-19: the phase 2b part of a randomized, placebo-controlled, phase 2/3 study. *Clin. Infect. Dis.* 76, 1403–1411. <https://doi.org/10.1093/cid/ciac933>.
- Culas, R., Nath, S., and Nath, S. (2023). Safely Prescribing Nirmatrelvir and Ritonavir-Avoiding Drug-Drug Interactions. *JAMA Intern. Med.* 183, 362–363. <https://doi.org/10.1001/jamainternmed.2022.6834>.
- Anderson, A.S., Cabel, P., and Rusnak, J.M.; EPIC-HR Trial Investigators (2022). Nirmatrelvir-Ritonavir and Viral Load Rebound in Covid-19. *N. Engl. J. Med.* 387, 1047–1049. <https://doi.org/10.1056/NEJMc2205944>.
- Charness, M.E., Gupta, K., Stack, G., Strymish, J., Adams, E., Lindy, D.C., Mohri, H., and Ho, D.D. (2022). Rebound of SARS-CoV-2 Infection after Nirmatrelvir-Ritonavir Treatment. *N. Engl. J. Med.* 387, 1045–1047. <https://doi.org/10.1056/NEJMc2206449>.
- Park, J.J., Lee, J., Seo, Y.B., and Na, S.H. (2022). Nirmatrelvir/Ritonavir Prescription Rate and Outcomes in Coronavirus Disease 2019: A Single Center Study. *Infect. Chemother.* 54, 757–764. <https://doi.org/10.3947/ic.2022.0123>.
- Heilmann, E., Costacurta, F., Moghadasi, S.A., Ye, C., Pavan, M., Bassani, D., Volland, A., Ascher, C., Weiss, A.K.H., Bante, D., et al. (2023). SARS-CoV-2 3CL(pro) mutations selected in a VSV-based system confer resistance to nirmatrelvir, ensitrelvir, and GC376. *Sci. Transl. Med.* 15, eabq7360. <https://doi.org/10.1126/scitranslmed.abq7360>.
- Dias, M.C., Pinto, D.C.G.A., and Silva, A.M.S. (2021). Plant Flavonoids: Chemical Characteristics and Biological Activity. *Molecules* 26, 5377. <https://doi.org/10.3390/molecules26175377>.
- Koes, R., Verweij, W., and Quattrocchio, F. (2005). Flavonoids: a colorful model for the regulation and evolution of biochemical pathways. *Trends Plant Sci.* 10, 236–242. <https://doi.org/10.1016/j.tplants.2005.03.002>.
- Erica, L.S., Beatriz Helena, L.N.S.M., Aurea, P.F., and Sirlei Dias, T. (2017). Flavonoids: Classification, Biosynthesis and Chemical Ecology. In *InTechOpen, Ch. 1*, C.J. Flavonoids, ed.. <https://doi.org/10.5772/67861>.
- Nguyen, T.T.H., Woo, H.J., Kang, H.K., Nguyen, V.D., Kim, Y.M., Kim, D.W., Ahn, S.A., Xia, Y., and Kim, D. (2012). Flavonoid-mediated inhibition of SARS coronavirus 3C-like protease expressed in *Pichia pastoris*. *Biotechnol. Lett.* 34, 831–838. <https://doi.org/10.1007/s10529-011-0845-8>.
- Alzaabi, M.M., Hamdy, R., Ashmawy, N.S., Hamoda, A.M., Alkhatay, F., Khademi, N.N., Al Joud, S.M.A., El-Keblawy, A.A., and Soliman, S.S.M. (2022). Flavonoids are promising safe therapy against COVID-19. *Phytochem. Rev.* 21, 291–312. <https://doi.org/10.1007/s11101-021-09759-z>.
- Jo, S., Kim, H., Kim, S., Shin, D.H., and Kim, M.S. (2019). Characteristics of flavonoids as potent MERS-CoV 3C-like protease inhibitors. *Chem. Biol. Drug Des.* 94, 2023–2030. <https://doi.org/10.1111/cbdd.13604>.
- Panche, A.N., Diwan, A.D., and Chandra, S.R. (2016). Flavonoids: an overview. *J. Nutr. Sci.* 5, e47. <https://doi.org/10.1017/jns.2016.41>.
- Zhang, L., Lin, D., Sun, X., Curth, U., Drosten, C., Sauerhering, L., Becker, S., Rox, K., and Hilgenfeld, R. (2020). Crystal structure of SARS-CoV-2 main protease provides a basis for design of improved alpha-ketoamide inhibitors. *Science* 368, 409–412. <https://doi.org/10.1126/science.abb3405>.
- Jiménez-Avalos, G., Vargas-Ruiz, A.P., Delgado-Pease, N.E., Olivos-Ramirez, G.E., Sheen, P., Fernández-Díaz, M., Quiliano, M., and Zimic, M.; COVID-19 Working Group in

- Perú (2021). Comprehensive virtual screening of 4.8 k flavonoids reveals novel insights into allosteric inhibition of SARS-CoV-2 M(Pro). *Sci. Rep.* 11, 15452. <https://doi.org/10.1038/s41598-021-94951-6>.
23. Fink, E.A., Bardine, C., Gahbauer, S., Singh, I., White, K., Gu, S., Wan, X., Ary, B., Glenn, I., O'Connell, J., et al. (2022). Large library docking for novel SARS-CoV-2 main protease non-covalent and covalent inhibitors. Preprint at bioRxiv. <https://doi.org/10.1101/2022.07.05.498881>.
 24. Chen, Y.C. (2015). Beware of docking. *Trends Pharmacol. Sci.* 36, 78–95. <https://doi.org/10.1016/j.tips.2014.12.001>.
 25. Jo, S., Kim, S., Shin, D.H., and Kim, M.S. (2020). Inhibition of SARS-CoV 3CL protease by flavonoids. *J. Enzyme Inhib. Med. Chem.* 35, 145–151. <https://doi.org/10.1080/14756366.2019.1690480>.
 26. Yonekura-Sakakibara, K., Higashi, Y., and Nakabayashi, R. (2019). The Origin and Evolution of Plant Flavonoid Metabolism. *Front. Plant Sci.* 10, 943. <https://doi.org/10.3389/fpls.2019.00943>.
 27. Wang, S., Alseekh, S., Fernie, A.R., and Luo, J. (2019). The Structure and Function of Major Plant Metabolite Modifications. *Mol. Plant* 12, 899–919. <https://doi.org/10.1016/j.molp.2019.06.001>.
 28. Trott, O., and Olson, A.J. (2010). AutoDock Vina: improving the speed and accuracy of docking with a new scoring function, efficient optimization, and multithreading. *J. Comput. Chem.* 31, 455–461. <https://doi.org/10.1002/jcc.21334>.
 29. Kuzikov, M., Costanzi, E., Reinshagen, J., Esposito, F., Vangeel, L., Wolf, M., Ellinger, B., Claussen, C., Geisslinger, G., Corona, A., et al. (2021). Identification of Inhibitors of SARS-CoV-2 3CL-Pro Enzymatic Activity Using a Small Molecule in Vitro Repurposing Screen. *ACS Pharmacol. Transl. Sci.* 4, 1096–1110. <https://doi.org/10.1021/acspstci.0c00216>.
 30. Feng, J., Li, D., Zhang, J., Yin, X., and Li, J. (2022). Crystal structure of SARS-CoV 3C-like protease with baicalein. *Biochem. Biophys. Res. Commun.* 611, 190–194. <https://doi.org/10.1016/j.bbrc.2022.04.086>.
 31. Liu, H., Ye, F., Sun, Q., Liang, H., Li, C., Li, S., Lu, R., Huang, B., Tan, W., and Lai, L. (2021). Scutellaria baicalensis extract and baicalein inhibit replication of SARS-CoV-2 and its 3C-like protease in vitro. *J. Enzyme Inhib. Med. Chem.* 36, 497–503. <https://doi.org/10.1080/14756366.2021.1873977>.
 32. Guerra, Y., Celi, D., Cueva, P., Perez-Castillo, Y., Giampieri, F., Alvarez-Suarez, J.M., and Tejera, E. (2022). Critical Review of Plant-Derived Compounds as Possible Inhibitors of SARS-CoV-2 Proteases: A Comparison with Experimentally Validated Molecules. *ACS Omega* 7, 44542–44555. <https://doi.org/10.1021/acsomega.2c05766>.
 33. Su, H.X., Yao, S., Zhao, W.F., Li, M.J., Liu, J., Shang, W.J., Xie, H., Ke, C.Q., Hu, H.C., Gao, M.N., et al. (2020). Anti-SARS-CoV-2 activities in vitro of Shuanghuanglian preparations and bioactive ingredients. *Acta Pharmacol. Sin.* 41, 1167–1177. <https://doi.org/10.1038/s41401-020-0483-6>.
 34. Ding, B., Ding, Q., Zhang, S., Jin, Z., Wang, Z., Li, S., and Dou, X. (2019). Characterization of the anti-Staphylococcus aureus fraction from Penthorum chinense Pursh stems. *BMC Complement. Altern. Med.* 19, 219. <https://doi.org/10.1186/s12906-019-2632-3>.
 35. Huang, D., Jiang, P., Chen, W., Yao, F., and Sun, L. (2014). Polyphenols with anti-proliferative activities from Penthorum chinense Pursh. *Molecules* 19, 11045–11055. <https://doi.org/10.3390/molecules190811045>.
 36. Zhang, T.T., Xu, X.L., Jiang, M.H., and Jiang, J.G. (2013). Hepatoprotective function of Penthorum chinense Pursh. *Food Funct.* 4, 1581–1585. <https://doi.org/10.1039/c3fo60245a>.
 37. Wang, M., Firman, J., Liu, L., and Yam, K. (2019). A Review on Flavonoid Apigenin: Dietary Intake, ADME, Antimicrobial Effects, and Interactions with Human Gut Microbiota. *BioMed Res. Int.* 2019, 7010467. <https://doi.org/10.1155/2019/7010467>.
 38. Tang, D., Chen, K., Huang, L., and Li, J. (2017). Pharmacokinetic properties and drug interactions of apigenin, a natural flavone. *Expert Opin. Drug Metab. Toxicol.* 13, 323–330. <https://doi.org/10.1080/17425255.2017.1251903>.
 39. Shankar, E., Goel, A., Gupta, K., and Gupta, S. (2017). Plant flavone apigenin: An emerging anticancer agent. *Curr. Pharmacol. Rep.* 3, 423–446. <https://doi.org/10.1007/s40495-017-0113-2>.
 40. Chaves, O.A., Fintelman-Rodrigues, N., Wang, X., Sacramento, C.Q., Temerozo, J.R., Ferreira, A.C., Mattos, M., Pereira-Dutra, F., Bozza, P.T., Castro-Faria-Neto, H.C., et al. (2022). Commercially Available Flavonols Are Better SARS-CoV-2 Inhibitors than Isoflavone and Flavones. *Viruses* 14, 1458. <https://doi.org/10.3390/v14071458>.
 41. Huang, S., Liu, Y., Zhang, Y., Zhang, R., Zhu, C., Fan, L., Pei, G., Zhang, B., and Shi, Y. (2020). Baicalein inhibits SARS-CoV-2/VSV replication with interfering mitochondrial oxidative phosphorylation in a mPTP dependent manner. *Signal Transduct. Target. Ther.* 5, 266. <https://doi.org/10.1038/s41392-020-00353-x>.
 42. Song, J., Zhang, L., Xu, Y., Yang, D., Zhang, L., Yang, S., Zhang, W., Wang, J., Tian, S., Yang, S., et al. (2021). The comprehensive study on the therapeutic effects of baicalein for the treatment of COVID-19 in vivo and in vitro. *Biochem. Pharmacol.* 183, 114302. <https://doi.org/10.1016/j.bcp.2020.114302>.
 43. Rudrapal, M., Issahaku, A.R., Agoni, C., Bendale, A.R., Nagar, A., Soliman, M.E.S., and Lokwani, D. (2022). In silico screening of phytopolyphenolics for the identification of bioactive compounds as novel protease inhibitors effective against SARS-CoV-2. *J. Biomol. Struct. Dyn.* 40, 10437–10453. <https://doi.org/10.1080/07391102.2021.1944909>.
 44. Mishra, G.P., Bhadane, R.N., Panigrahi, D., Amawi, H.A., Asbhy, C.R., Jr., and Tiwari, A.K. (2021). The interaction of the bioflavonoids with five SARS-CoV-2 proteins targets: An in silico study. *Comput. Biol. Med.* 134, 104464. <https://doi.org/10.1016/j.compbiomed.2021.104464>.
 45. Imran, M., Iqbal, S., Hussain, A., Uddin, J., Shahzad, M., Khaliq, T., Razaq Ahmed, A., Mushtaq, L., Kashif, M., and Mahmood, K. (2022). In silico screening, SAR and kinetic studies of naturally occurring flavonoids against SARS CoV-2 main protease. *Arab. J. Chem.* 15, 103473. <https://doi.org/10.1016/j.arabjc.2021.103473>.
 46. Al-Karmalawy, A.A., Farid, M.M., Mostafa, A., Ragheb, A.Y., S. H.M., Shehata, M., Shama, N.M.A., GabAllah, M., Mostafa-Hedeab, G., and Marzouk, M.M. (2021). Naturally Available Flavonoid Aglycones as Potential Antiviral Drug Candidates against SARS-CoV-2. *Molecules* 26, 6559. <https://doi.org/10.3390/molecules26216559>.
 47. Chen, D.Y., Khan, N., Close, B.J., Goel, R.K., Blum, B., Tavares, A.H., Kenney, D., Conway, H.L., Ewoldt, J.K., Chitalia, V.C., et al. (2021). SARS-CoV-2 Disrupts Proximal Elements in the JAK-STAT Pathway. *J. Virol.* 95, e0086221. <https://doi.org/10.1128/JVI.00862-21>.
 48. Xiong, G., Wu, Z., Yi, J., Fu, L., Yang, Z., Hsieh, C., Yin, M., Zeng, X., Wu, C., Lu, A., et al. (2021). ADMETlab 2.0: an integrated online platform for accurate and comprehensive predictions of ADMET properties. *Nucleic Acids Res.* 49, W5–W14. <https://doi.org/10.1093/nar/gkab255>.
 49. Shrum, B., Anantha, R.V., Xu, S.X., Donnelly, M., Haeryfar, S.M.M., McCormick, J.K., and Mele, T. (2014). A robust scoring system to evaluate sepsis severity in an animal model. *BMC Res. Notes* 7, 233. <https://doi.org/10.1186/1756-0500-7-233>.

STAR★METHODS

KEY RESOURCES TABLE

REAGENT or RESOURCE	SOURCE	IDENTIFIER
Antibodies		
Anti-SARS-CoV nucleocapsid antibody	Rockland	200-401-A50; RRID: AB_828403
AlexaFluor 568-conjugated goat anti-rabbit secondary antibody	ThermoFisher Scientific	A-11011; RRID:AB_2925778
Bacterial and virus strains		
BL21(DE3) pLysS Competent Cells	Sigma	69451
2019-nCoV/USA-WA1/2020	Centers for Disease Control and Prevention and BEI Resources	NCBI accession number MN985325
Chemicals, peptides, and recombinant proteins		
DabcyL-KTSAVLQSGFRKM-E(Edans)-NH2	GL Biochem	Custom Synthesis
Roche cOmplete His-Tag Purification Resin	Sigma	5893801001
PreScission protease	Sigma	GE27-0843-01
NdeI	New England BioLabs	R0111
BamHI	New England BioLabs	R0136
Isopropyl β-D-thiogalactopyranoside	Gold Biotechnology	I2481C100
Flavonoid Library	Wuhan ChemFaces Biochemical Co.	S30005
Dithiothreitol	Sigma	D0632
Tris-HCl		
NaCl		
EDTA		
Dulbecco's modified Eagle Medium (DMEM)	Gibco	11995-065
Heat-inactivated fetal bovine serum		
Paraformaldehyde, 8% w/v aqueous solution, methanol-free	Thermo Scientific	047347.9M
DPBS, no calcium, no magnesium	Gibco	14190144
4',6-diamidino-2-phenylindole dihydrochloride(DAPI)	Thermo Scientific	62247
Lipopolysaccharide (LPS) from <i>E. coli</i> serotype O111:B4	Sigma	L2630
Experimental models: Cell lines		
African green monkey kidney Vero E6 cells	ATCC	CCL-81
Recombinant DNA		
pET-15b	Sigma	69661
Software and algorithms		
Prism	Graphpad by Dotmatics	https://www.graphpad.com/features
ImageJ	NIH and LOCI, University of Wisconsin	https://imagej.nih.gov/ij/download.html
Autodock Vina	Scripps Research Institute	http://vina.scripps.edu/
Chimera	UCSF	https://www.cgl.ucsf.edu/chimera/download.html
PyMol	Schrodinger	https://pymol.org/2/
Smina		https://sourceforge.net/projects/smina
GROMACs version 2020.6	Uppsala University, University of Groningen	GPL versions

RESOURCE AVAILABILITY

Lead contact

Further information and requests for resources and reagents should be directed to the lead contact and corresponding author, Robert Flaumenhaft. (rflaumen@bidmc.harvard.edu).

Materials availability

All reagents generated in this study are available from the corresponding author with a completed Materials Transfer Agreement.

Data and code availability

- The published article and supplemental information include all data generated and analyzed during this study.
- This paper does not report original code.
- Any additional information required to analyze the data reported in this paper is available from the [lead contact](#) upon request.

EXPERIMENTAL MODEL AND STUDY PARTICIPANT DETAILS

Biocontainment

The SARS-CoV-2 infection experiments were carried out in a state-of-the-art biosafety level 3 (BSL3) facility at the National Emerging Infectious Diseases Laboratories (NEIDL) of Boston University using biosafety protocols approved by the Institutional Biosafety Committee (IBC) that comprises scientists, biosafety and compliance experts as well as local community members. The biosafety protocols were further approved by the Boston Public Health Commission. All personnel received rigorous biosafety, biosecurity, and BSL3 training before participating in experiments. Special personal protective equipment, including scrubs, disposable overalls, shoe covers, double-layered gloves, and powered air-purifying respirators, was used during BSL3 work.

METHOD DETAILS

Mpro expression and purification

The gene encoding SARS-CoV-2 Mpro containing the Mpro cleavage-site (SAVLQ↓SGFRK) at the N-terminus and a PreScission cleavage site (SGVTFQ↓GP) at the C-terminus was cloned between the NdeI and BamHI restriction enzyme site in a pET-15b expression vector. The vector was transformed into *Escherichia coli* Rosetta (DE3) pLysS (Novagen) and grown in LB-ampicillin broth at 37°C. Expression of the His-tagged Mpro was induced with 0.5 mM isopropyl β-D-1-thiogalactopyranoside (IPTG) overnight at 23°C. The cells were harvested by centrifugation and were lysed with a lysis buffer and by sonication. The lysate was clarified by centrifugation and was mixed with Roche cComplete His-Tag Purification Resin (Roche) for capturing the protein. The captured protein was treated with PreScission protease to remove the His-tag and the released Mpro was further purified through a Superdex 75 column with fast protein liquid chromatography (FPLC).

High-throughput screening of the flavonoid library

A compound library that contains 1019 flavonoids (Wuhan ChemFaces Biochemical Co., Ltd.) was screened at the ICCB-Longwood Screening Facility at Harvard Medical School. Monitoring SARS-CoV-2 Mpro enzymatic activity was performed as previously described⁴ using Förster resonance energy transfer (FRET) to observe the cleavage of a peptide substrate containing the Mpro cleavage site (Dabcyl-KTSAWLQ↓SGFRKM-EDANS (GL Biochem, Shanghai)). For the high-throughput screening assay, 17 μM of the compounds were mixed with 50 nM Mpro in a Tris buffer (20 mM Tris, NaCl 100 mM, DTT 5 mM, pH 7.5) for 30 min prior to the addition of 7.5 μM peptide substrate. The enzymatic activity was monitored for fluorescence of the peptide (ex:360; em460) for 30 min. IC₅₀ data was plotted as the percentage of Mpro activity (V_{max}) inhibition in the absence of inhibitors versus inhibitor concentration and fit to the following equation using GraphPad Prism v9 (La Jolla, CA, USA).

$$\% \text{ MPro Activity Inhibition} = \left(\frac{100}{1 + \frac{[\text{Flavonoid}]}{IC_{50}}} \right)$$

Mpro activity assays

For the Mpro fluorescence-based activity assay, 50 nM Mpro was treated with varying concentrations of flavonoids in a tris buffer (20 mM tris, 100 mM NaCl, 0.5 mM EDTA buffer containing 5 mM DTT, pH 7.5) for 30 min at room temperature prior to the addition of 7.5 μM of the Dabcyl-KTSAWLQ↓SGFRKM-EDANS peptide. EDANS fluorescence is quenched by Dabcyl in the intact peptide whereas cleavage of the peptide between Gln and Ser will produce a fluorescent product at 340 nm excitation and 460 nm emission.

To test for inhibitor reversibility, 300 μM flavonoid was incubated with 15 nM Mpro for 30 min at room temperature followed by dilution of the inhibitor to 6 μM with Tris buffer. The reaction mixture was initiated with 7.5 μM of the peptide substrate followed by a continuous fluorescent read of the enzymatic activity. Irreversibility by the flavonoid was determined by its ability to maintain enzyme inhibition post-dilution.

For the mass spectrometry-based substrate cleavage assay, 200 nM Mpro was incubated with 25 μ M of flavonoid and 20 μ M Dabcyl-KTSAWLQ↓SGFRKM-EDANS in a tris buffer (20 mM Tris, 100 mM NaCl, pH 8.0) for 3 h at room temperature. Mass spectrometry of the cleaved products was performed at the Taplin Biological Mass Spectrometry Facility at Harvard Medical School.

Immunofluorescence of SARS-CoV-2 viral replication

Immunofluorescence of virus-infected cells was performed as previously described.⁴⁷ Briefly, African green monkey kidney Vero E6 cells grown to ~80% confluence were treated with compounds for 2 h prior to infection. The SARS-CoV-2 USA-WA1/2020 isolate (NCBI accession number: MN985325) was directly added to the culture medium in the presence of compounds, followed by 24 h incubation at 37°C, after which the cells were fixed in 4% v/v paraformaldehyde for 30 min. The cells were washed with 1x phosphate buffered saline (PBS), permeabilized, and incubated with an anti-SARS-CoV nucleocapsid antibody (Rockland) at 1:2000 dilution. Excess primary antibody was washed away with PBS prior to further staining with an AlexaFluor 568-conjugated goat anti-rabbit secondary antibody (ThermoFisher Scientific) at 1:1000 dilution for 1 h in the dark. Finally, the cells were counterstained with 4',6-diamidino-2-phenylindole (DAPI) to visualize the nucleus. The cells were imaged in an EVOS M5000 imaging system (ThermoFisher Scientific). Quantification was performed on a MuviCyte live-cell imaging system (PerkinElmer, Waltham, MA) by determining viral antigen-positive cells per DAPI-positive cells. The percentage of DAPI-stained cells showing viral antigen was plotted with mean \pm standard deviation (SD) of multiple images.

Molecular docking

Docking studies were carried out using Autodock Vina. Docking was performed to obtain a population of possible conformations and orientations for the ligand at the binding site. The protein was converted to PDBQT file that contains a protein structure with hydrogens in all polar residues. All bonds of ligands were set as rotatable. All calculations for the protein-fixed ligand-flexible docking were done using the Lamarckian Genetic algorithm (LGA) method. The best conformation was chosen with the lowest binding energy after the docking search was completed. The interactions of protein-ligand conformations, including hydrogen bonds and the bond lengths, were analyzed using Chimera and PyMol. PDB: 7B3E and PubChem: 5281600 were used for the myricetin bound main protease (3CLpro/Mpro) cocrystal structure and the three-dimensional structure of amentoflavone, respectively.

Molecular dynamics simulation

For investigating the interaction of PGHG with SARS-COV-2 Mpro, Smina (v2021-08-23) was used for molecular docking of PGHG with SARS-COV-2 Mpro to obtain possible conformations and orientations of ligands at binding sites. The crystal structure (PDB: 7B3E) of SARS-COV-2 Mpro was used as the receptor. The ligand in 7B3E was used to locate the binding site of Mpro (ligand_autobox). A conformation search algorithm was performed to explore the conformational states of a flexible ligand, using grid maps to evaluate the ligand-protein interaction at each point in the docking simulation. The docking results were clustered to identify similar conformations. The conformation with the lowest binding free energy was finally identified as the best probable conformation. MD simulation was performed in GROMACS (version 2020.6) for the complex of PGHG with SARS-COV-2 Mpro. AMBER 03 Force Field and General AMBER Force Field (GAFF) parameters were used for the protein and ligand molecule, respectively. The partial atomic charges of the ligand were calculated by the restrained electrostatic potential (RESP) charge following the optimization of ligand at B3LYP/6-31G(d) level by Gaussian16 package. The complex was then solvated with simple point-charge (SPC) water molecules in a box at 1.2 nm solvated layer. The particle mesh Ewald (PME) method was employed to treat the long-range electrostatic interactions and the calculated radius of van der Waals interaction was 1.2 nm. Before the production run, the systems were relaxed by 1000 steps using the steepest descent algorithm followed by other 1000 steps using the conjugate gradient method. For the equilibration phase, the temperature and the pressure were controlled by using the Berendsen coupling algorithm with a time constant of 0.1 and 1.0 ps, respectively. For the production run, an integration time step of 2 fs was employed to integrate the equations of motion. The Parrinello-Rahman coupling algorithm was used to keep the pressure constant. The simulated temperature was set to 298.15 K and 200 ns molecular dynamics simulation was performed in the NPT ensemble. The binding free energy of receptor–ligand complex was calculated with gmx_MMPBSA (version 1.5.7) based on MMPBSA.py from AmberTools20 suit.

Endotoxemia Model

8–12 weeks old C57Bl/6J mice were administered 10 μ g/g LPS from *E. coli* serotype 0111:B4 intraperitoneally in the presence of 5 μ g/g PGHG or DMSO as the vehicle control. The dose was selected based on a calculated volume of distribution for PGHG of 0.31⁴⁸ to result in a plasma concentration of ~18 μ M. The mice were monitored for up to 12 h using a 7-parameter murine sepsis scoring system.⁴⁹ The following variables were scored on a scale of 0–4: appearance, level of consciousness, activity, response to stimulus, condition of eyes, respiratory rate, and respiratory quality. Mice were analyzed in a blinded fashion and included a vehicle control cohort (N = 4) and a 5 μ g/g PGHG cohort (N = 4). The data was analyzed by one-way ANOVA and a p-value of <0.05 was considered statistically significant. Data represented as mean \pm SEM.

QUANTIFICATION AND STATISTICAL ANALYSIS

Statistics were performed with GraphPad Prism 9 on individual experiments as indicated.